Hydrogen-bonded one-dimensional molecular chains on ultrathin insulating films: Quinacridone on KCl/Cu(111)

Rémi Bretel, Séverine Le Moal, Hamid Oughaddou, and Eric Le Moal [*]
Université Paris-Saclay, CNRS, Institut des Sciences Moléculaires d'Orsay, 91405 Orsay, France

We report on the growth of one-dimensional (1D) chains of the prochiral quinacridone (QA) molecule on ultrathin KCl films on Cu(111) in ultrahigh vacuum. Using low-temperature scanning tunneling microscopy (STM), we observe straight homochiral 1D chains of QA molecules on one (1L), two (2L), and three (3L) atomic layer thick (100)-terminated KCl islands. The KCl films mostly consist of 2L-thick KCl islands delineated by long polar and short nonpolar edges. These 2L-thick KCl islands are topped by smaller one-atom-thick KCl islands or pits, which are delineated by nonpolar step edges. We find that QA chains can nucleate at these nonpolar step edges or on top of KCl terraces without assistance of step edges. In both cases, the longest straight QA chains observed grow along the KCl ⟨100⟩ directions or slightly rotated (typically less than 10°) from them. Intermolecular distances ranging from 6.4 Å to 6.8 Å are measured for QA chains on KCl/Cu(111), which is compatible with hydrogen bonds between neighboring flat-lying QA molecules. These intermolecular distances being larger than the measured KCl lattice parameter (i.e., 6.21 Å at 78 K), QA chain growth on KCl/Cu(111) is incommensurate. Molecular arrangement models for the QA chains on KCl are proposed, based on the analysis of the STM images.

I. INTRODUCTION

Molecular self-assembly on surfaces is a unique bottom-up fabrication technique, which has been increasingly used to grow artificial one- and two-dimensional (1D/2D) supramolecular architectures with emergent physical and chemical properties [1–5]. This fabrication technique relies on the spontaneous (or temperature-activated) organization of adsorbed molecules into well-defined, stable or metastable, periodic arrangements through a delicate balance of intermolecular and molecule-substrate interactions [6–8]. It opens up new prospects not only for fundamental research in interfaces and materials science, but also for the development of novel industrial processes and device technology [9–12]. Recently, linear chains of hydrogen-bonded organic molecules have raised a considerable research effort, because they are considered ideal platforms for the study of electronic and excitonic effects in quantum-confined molecular systems [13–15]. Furthermore, such 1D molecular chains may become ultimate excitonic nanowires in future nanotechnologies using charge-neutral molecular excitations as the information vector [16–23].

The growth of hydrogen-bonded 1D chains of various molecules on metals has already been reported [24–31], including quinacridone (QA) on Ag(111) [32], Ag(100) and Cu(111) [33], and on the semimetal HOPG [34]. Low-energy electron diffraction (LEED) and scanning tunneling microscopy (STM) studies have shown that the growth of such 1D molecular chains on metals can be controlled through the substrate temperature and the coverage rate. However, on

the one hand, hybridization of the molecular orbitals and the metal surface states due to direct adsorption on the metal strongly alters the excitonic properties of the molecules [35]. On the other hand, the use of insulating substrates prevents the use of surface science tools based on charged particles, such as LEED and STM. In the context of single-molecule spectroscopy, this problem has been solved by the use of ultrathin insulating films of alkali halides [36,37]. For instance, the intrinsic luminescence of individual molecules has been measured using STM-induced luminescence [38–41] and STM tip-enhanced photoluminescence spectroscopy [42–44] on ultrathin NaCl films grown on silver and gold crystal surfaces. Ultrathin films of KCl have also been used to electronically decouple organic nanocrystals [45,46] and molecular layers [47] from silver and gold surfaces for STM-based experiments. However, the growth of hydrogen-bonded molecular chains on ultrathin alkali-halide films is still a challenge.

The difficulty arises from the high surface mobility of the molecules on alkali halides and the nonideal growth mode of alkali-halide thin films. At low surface coverages, on most metal surfaces, alkali-halide thin films consist of isolated islands, around which the substrate surface is bare [48–51]. Though the mobility of the molecules is required for their self-assembly, it often yields that all the molecules migrate onto the bare metal areas. In several recent studies, this issue was circumvented by the manipulation of single molecules using the tip of an STM, to assemble them in a row [40,52]. In such a method, the length of the chains and the number of chains may be strongly limited. So far, self-assembled, hydrogen-bonded 1D chains of molecules on ultrathin insulating films have never been reported.

In this article, we report the self-assembly of hydrogen-bonded 1D chains of quinacridone (QA) molecules on

---

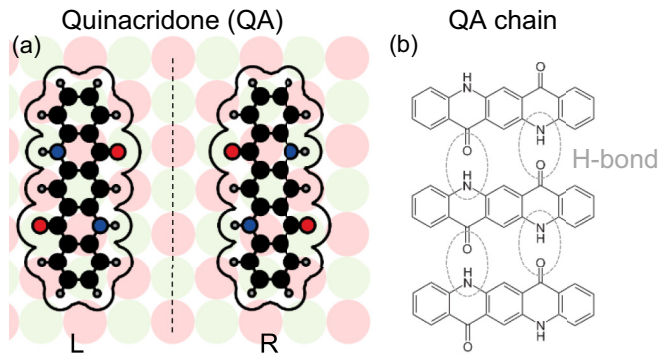*eric.le-moal@universite-paris-saclay.fr

Quinacridone (QA)

QA chain

FIG. 1. Quinacridone (QA), molecular formula: $C_{20}H_{12}N_2O_2$. (a) Hard-sphere model and van der Waals radii [33] of the linear *trans*-isomer of QA, lying flat on a KCl(100) surface. The molecule is a prochiral molecule; i.e., depending on which of its two faces the molecule adsorbs on a surface, it is one or the other of the two enantiomers (L or R) shown in the figure. The atoms in the QA model are carbon (black), hydrogen (gray), nitrogen (blue), and oxygen (red). Here, the adsorption site of QA on KCl is arbitrary. (b) Structural formula of QA and schematic representation of a homochiral (i.e., enantiopure) QA chain, highlighting the hydrogen bonds between the neighboring molecules.

ultrathin KCl films epitaxially grown on Cu(111) in ultrahigh vacuum (UHV). The KCl films consist of (100)-terminated KCl islands, whose thickness ranges from one (1L) to three (3L) atomic layers. The linear *trans*-isomer of QA is a prochiral molecule, as shown in Fig. 1(a). This molecule is known to self-assemble in hydrogen-bonded 1D chains [53,54], as shown in Fig. 1(b). The model system QA/KCl/Cu(111) is both of fundamental and technological interest, because QA is actively considered for future organic-based electronic and optoelectronic devices [54–59] and alkali-halide thin films are increasingly used as buffer layers at the electrode/semiconductor interfaces to enhance the performance of such devices [60–67]. Using low-temperature STM, we observe straight homochiral QA chains grown on KCl islands. First, we describe the epitaxial growth of KCl on Cu(111), which has rarely been considered so far [68]. Ultrathin KCl film growth on Cu(111) exhibits some structural characteristics that it does not have on other metal and semiconductor surfaces studied so far, i.e., on Au(111) [47,69], Ag(100) [70], stepped Cu surfaces [71,72], and Si(111) [73]. Then, we determine the in-plane orientation of the QA chains relative to the main crystal axes of the Cu(111) substrate and the KCl(100) islands. We measure the intermolecular distances in the QA chains on KCl/Cu(111). Finally, the (L or R) enantiomers are identified and the in-plane orientation of the molecules relative to the chain axis is determined from the STM images, in order to propose molecular arrangement models for the observed QA chains on KCl/Cu(111).

II. METHODS

All experiments are carried out in ultrahigh vacuum (UHV). STM measurements are conducted at a base pressure of less than 1×10^{-10} mbar using a low-temperature STM (Scienta Omicron, Uppsala) operated at 78 K (liquid nitrogen

cryostat) in the constant current mode. The STM tip is an electrochemically etched tungsten wire. The substrate is a Cu(111) single crystal (SPL, Zaandam), which we clean in UHV through cycles of sputtering with Ar^+ ions (800 eV, 10 μA, 60 minutes) and annealing at 673 K for 15 minutes. We deposit QA and KCl molecules by thermal evaporation of QA powder purified by sublimation and $\geqslant 99.9995\%$-pure KCl powder (Sigma Aldrich), using a water-cooled evaporator equipped with quartz crucibles (TCE-CS, Kentax, Seelze), at cell temperatures of 553 to 573 K for QA and 803 to 813 K for KCl. The results shown in this article are obtained by depositing KCl and QA on the copper crystal about 5 minutes after the sample is taken out of the low-temperature STM. Thus, the temperature of the substrate at the start of KCl and QA deposition is intermediate between the temperature measured in the STM (78 K) and the temperature measured at the sample holder (303 K). KCl deposition on Cu(111) at low temperature makes it possible to obtain 1L- to 3L-thick KCl islands and to avoid the formation of thicker islands (possibly by increasing the nucleation rate and limiting dewetting effects). Cooling the KCl/Cu(111) sample before QA deposition favors the growth of QA chains on KCl islands, presumably because this slows down the diffusion of QA molecules out of the KCl islands toward the uncovered Cu(111) areas, as compared to room temperature [74,75]. All STM image analysis is performed using the Gwyddion [76] and ImageJ [77] softwares. In order to compensate for the lateral drift of the sample, the STM tip is scanned across the sample back and forth and the distances are measured on the four resulting images (i.e., trace and retrace, up and down). The uncertainty on the measured distances is evaluated from the dispersion of the values obtained from these four images. The Z-scanner of the STM is calibrated using the Cu(111) atomic step height $h_{Cu(111)}$, which we measure on the clean Cu(111) sample. The theoretical value of this step height ($h_{Cu(111)} \approx 208.7$ pm) is calculated using the lattice parameter of copper ($a_{Cu} = 361.5$ pm at 297 K) and the relation $h_{Cu(111)} = \frac{a_{Cu}}{\sqrt{3}}$.

III. RESULTS AND DISCUSSION

In Sec. III A, we describe the growth of ultrathin KCl films on Cu(111). In Sec. III B, we determine the adsorption model of the QA chains on KCl and we infer the role of QA-QA and QA-KCl interactions in the growth of these chains.

A. Ultrathin KCl films on Cu(111)

Figure 2 shows STM images of ultrathin KCl films grown on Cu(111) using two different sets of preparation conditions, in order to obtain various film thicknesses. In Figs. 2(a) and 2(b), KCl is deposited for 5 minutes at a cell temperature of 813 K and for 10 minutes at 803 K in Figs. 2(c) to 2(e). The number of atomic layers in the KCl islands is estimated on the basis of their STM heights and of comparisons with the STM heights of NaCl islands grown on Cu(111).

At a sample bias of 4.0 V and a set-point current of 4 pA, we measure STM heights of 229 ± 24 pm and 398 ± 36 pm relative to the Cu(111) surface, for the 1L- and 2L-thick KCl islands. In these STM images, the one-atom-thick areas found on top of these 1L- and 2L-thick KCl islands have apparent
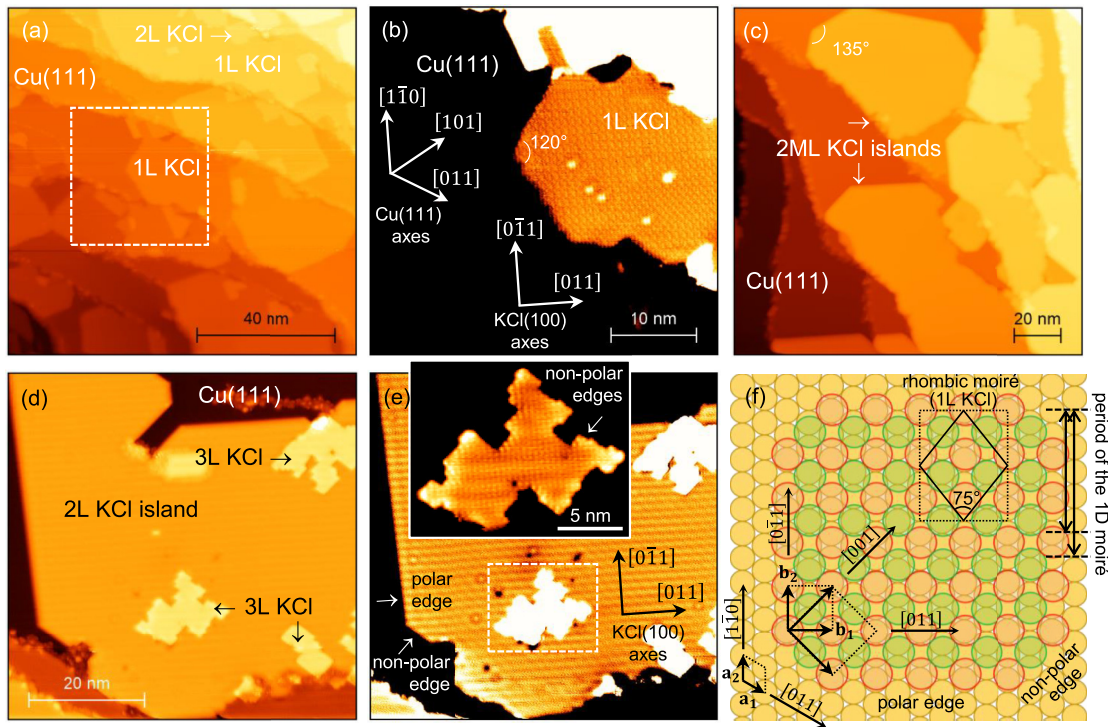
FIG. 2. (a)–(e) STM topography images of ultrathin KCl films grown on Cu(111) featuring one (1L), two (2L), and three (3L) atomic layer thick areas. STM parameters: (a), (b) sample bias 4.0 V, set-point current 10 pA; (c) 4.0 V, 30 pA; (d), (e) 3.0 V, 4 pA. (a) 1L-thick KCl islands featuring a few 2L-thick KCl domains and surrounded by noncovered Cu(111) areas. (b) Same area as framed in dotted line in (a). The color scale covers a narrow height range, in order to highlight the moiré pattern in the 1L-thick KCl area. The axes shown in this image indicate the main crystal directions of the Cu(111) surface and of the (100) plane of the considered KCl island. (c) 2L-thick KCl islands. (d) 2L-thick KCl island featuring a few 3L-thick KCl domains. (e) Same area as (d), with adapted height scale to highlight the moiré pattern in the 2L-thick KCl area. In inset, the area framed in dotted line is shown with adapted height scale to highlight the moiré pattern and the atomic resolution in the 3L-thick KCl area. (f) Atomic model for the 2L-thick (100)-terminated KCl islands on Cu(111), oriented with one of the ⟨011⟩ directions of the KCl(100) plane parallel to one of the ⟨011⟩ directions of the Cu(111) plane.

thicknesses of 169 ± 12 pm and 139 ± 12 pm, respectively. Using the same STM parameters, we measure an STM height of 362 ± 12 pm for 2L-thick NaCl islands and an apparent thickness of 121 ± 6 pm for the one-atom-thick area growing on top of these islands, i.e., for the third NaCl layer (see the corresponding STM images in Fig. S1 of the Supplemental Material [78]). These observations are consistent with the fact that the lattice constant of KCl is about 10% larger than that of NaCl. We believe that this corroborates our assessment of the KCl layer thicknesses. No 1L-thick NaCl islands are observed on Cu(111) within the investigated growth conditions.

The orientation of the main crystal axes of the Cu(111) surface, as indicated in Fig. 2(b), and the nearest Cu-Cu interatomic distance at the temperature of the STM measurements (252 ± 1 pm at 78 K) are known from atomic-resolution STM images of the clean Cu(111). From Figs. 2(c) to 2(e), we learn that 2L-thick KCl islands are oriented with one of the KCl ⟨110⟩ directions parallel to one of the Cu ⟨110⟩ directions. A possible arrangement of the KCl atoms on the Cu(111) surface for this orientation of the KCl lattice is illustrated in Fig. 2(f). Based on this model, we hypothesize the following relation of epitaxy between the film and the substrate, where $(\mathbf{a_1}, \mathbf{a_2})$ and $(\mathbf{b_1}, \mathbf{b_2})$ are the vector bases of the primary cells of the Cu(111) and KCl(100) surfaces and we assume $\mathbf{b_2} \parallel \mathbf{a_2}$,

respectively:

$$\mathbf{b_1} = 2\mathbf{a_1} + \mathbf{a_2}. \tag{1}$$

From fast Fourier transform (FFT) of the atomic-resolution STM image shown in Fig. 2(e), we measure that the nearest Cl-Cl interatomic distance at 78 K equals 439 ± 1 pm. This corresponds to a ratio of the lattice parameters $|\mathbf{b_1}|/|\mathbf{a_1}| = 1.74 \pm 0.01$. To less than 1%, this ratio is the same as what is known for bulk KCl and Cu at room temperature [79]. Moreover, to the precision of the experiment, the measured ratio verifies the condition $|\mathbf{b_1}|/|\mathbf{a_1}| = \sqrt{3}$ required by Eq. (1), which confirms the epitaxial relationship proposed in Eq. (1). This coincidence of the KCl and Cu lattices only exists along the KCl ⟨110⟩ direction that is orthogonal to one of the Cu ⟨110⟩ directions. Perpendicularly to this direction, we observe a periodic modulation of the STM height, i.e., a one-dimensional (1D) moiré pattern. The period of this modulation is the same in the 2L-thick and 3L-thick areas of a given island; however, it differs from an island to another. The shortest and longest periods measured within the reported experiments are 1.29 ± 0.01 nm and 1.53 ± 0.01 nm, which is close to $n|\mathbf{a_2}|$ where $n = 5$ and $n = 6$, i.e., 1.260 ± 0.005 nm and 1.512 ± 0.006 nm at 78 K, respectively. Using the model shown in Fig. 2(f), we notice that these extremal values of

the period could correspond to the equations $3\mathbf{b_1} = 5\mathbf{a_2}$ and $\frac{7}{2}\mathbf{b_1} = 6\mathbf{a_2}$, which requires a contraction of the KCl lattice by about 5% and 2%, respectively. Since we do not measure such a contraction in the atomic-resolution STM images, we conclude that KCl growth on Cu(111) is incommensurable in this direction. The variability of the period of the observed 1D moiré pattern might result from different, undetected, subtle reconstruction of either the KCl film or Cu(111) surface, which are sufficiently similar in potential energy to coexist in the studied system. To sum up, a *point-on-line* coincidence is evidenced for the 2L- and 3L-thick KCl islands on Cu(111) that have one of the KCl ⟨110⟩ directions parallel to one of the Cu ⟨110⟩ directions.

Based on Figs. 2(c) to 2(e), we demonstrate that the 2L-thick KCl islands on Cu(111) are delineated by alternating long polar and short nonpolar edges, i.e., edges parallel to the KCl ⟨110⟩ and ⟨100⟩ directions, respectively. This unusual feature may result from the fact that KCl nonpolar edges are not aligned with any particular crystal direction of the Cu(111) surface, unlike the polar edges. As shown in Fig. 2(f), the KCl polar edges either are parallel to one of the Cu ⟨110⟩ directions or verify the epitaxial relationship defined in Eq. (1), which may be thermodynamically favorable. In contrast, the one-atom-thick KCl "islets" topping 2L-thick KCl islands feature only nonpolar edges, supposedly because their interaction with the underlying Cu(111) surface is comparatively much weaker. Only based on the results shown in Fig. 2, we cannot exclude that the presence of long polar edges results from the low substrate temperature during KCl deposition. However, a similar alternation of polar and nonpolar edges was previously observed for KCl islands grown on Cu(110) at room temperature and at 370 K [68].

As shown in Figs. 2(a) and 2(b), 1L-thick KCl islands on Cu(111) exhibit distinctive recognizable characteristics that 2L- and 3L-thick KCl islands do not have. A more intricate, two-dimensional (2D) moiré pattern is observed. The same moiré pattern is observed in 1L-thick areas corresponding to one-atom-thick pits in 2L-thick KCl islands. Because of this, and based on the symmetry of this moiré pattern, we deduce that 1L-thick KCl islands are (100)-terminated, like 2L- and 3L-thick islands, and we determine the in-plane orientation of the KCl axes, as shown in Fig. 2(b). The 2D moiré pattern found in 1L-thick KCl areas consists of a matrix of bright dots, which has a rectangular unit cell of dimensions $(883 \pm 5) \times (1130 \pm 5)$ pm. From these values, we deduce that the unit vectors of this moiré pattern equal $4\mathbf{a_1} + 2\mathbf{a_2}$ and $\frac{9}{2}\mathbf{a_2}$, respectively. As shown in Fig. 2(f), this moiré pattern could correspond to the relation of epitaxy defined by Eq. (1) along the direction of $\mathbf{b_1}$ and to the relation $5\mathbf{b_2} = 9\mathbf{a_2}$ along the direction of $\mathbf{b_2}$. These two relations imply a uniaxial expansion of the KCl lattice by about 3% along the $\mathbf{b_2}$ axis. We cannot experimentally confirm this expansion because the moiré pattern totally dominates over atomic resolution in the STM images. At positive sample bias, a smaller bright spot is visible at the center of the rectangular unit cell of the moiré pattern. Altogether, the (smaller or larger) bright spots mark the nodes of a rhombic lattice, whose acute angle equals 75°. In addition, we find that the 1L-thick KCl islands feature irregular (i.e., not straight) edges, which meet at angles of either 90°, 120°, or 135° [see, e.g., in Fig. 2(b)],

presumably because of the interaction with the underlying Cu(111) surface.

From our STM measurements, we find that the great majority of 2L-thick KCl islands on Cu(111) have the in-plane orientation described in Fig. 2, where one of the KCl ⟨110⟩ directions is parallel to one of the Cu ⟨110⟩ directions and a 1D moiré pattern is observed. However, a minority of 2L-thick KCl islands oriented with the KCl ⟨110⟩ directions at 15° from the Cu ⟨110⟩ directions is also found. In this case, a 2D moiré pattern, with spatial periods in the range of 0.9 to 1.1 nm, is observed. From our STM measurements (shown in the Supplemental Material [78]), we observe the same favored in-plane orientations of the QA chain axis relative to the KCl lattice, irrespective of the in-plane orientation of the KCl islands relative to the Cu(111) surface. This indicates that, from KCl thicknesses of 2L on, the Cu(111) surface has a negligible effect on the in-plane orientation of the QA chains grown on KCl/Cu(111). Therefore, in the next section, we focus on QA chain growth on KCl islands oriented as shown in Fig. 2.

B. QA chains on KCl/Cu(111) islands

1. QA chains on 1L-thick KCl

Figures 3 and 4 show STM images of QA molecules deposited on 1L- and 2L-thick KCl areas of KCl islands grown on Cu(111). We find that QA spontaneously arranges in 1D molecular chains both on bare Cu(111) and on KCl islands, as shown in Fig. 3(a). On KCl, most of the QA chains grow on the 1L-thick KCl areas and are connected to a nonpolar step edge between 1L- and 2L-thick KCl areas. In Fig. 3(b), we consider three straight QA chains on 1L-thick KCl, labeled from ① to ③. These chains comprise 14, 7, and 13 molecules, respectively. To the precision of the measurement, these three chains have the same in-plane orientation, i.e., with the chain axis at $+(2.5 \pm 1.0)°$ from the KCl [001] direction, and the same intermolecular distance. By autocorrelation of height profiles taken along the chain axis, we determine that neighboring molecules are separated by (634 ± 9) pm, (635 ± 9) pm, and (641 ± 7) pm in QA chains ①, ②, and ③, respectively. In the following, we use the STM images to determine the chirality of the QA molecules, i.e., whether they adsorb on KCl as the L or R enantiomer [as introduced in Fig. 1(a)], and their in-plane orientation with respect to the chain axis and the KCl directions.

At positive sample bias, the STM image of most QA molecules on 1L-thick KCl/Cu(111) exhibits a characteristic three-lobe geometry, which mirrors the partial density of states of the lowest unoccupied molecular orbital (LUMO), as calculated for the neutral molecule using density functional theory (DFT), as shown in Fig. 3(f). The same STM contrast has been previously reported for QA molecules on few-layer NaCl films on Ag(111) [41]. The partial density of states of the LUMO features two spherical lobes around the molecule ends and an S-shaped (or Ƨ-shaped) central lobe (depending on which enantiomer is considered). For the R(L)-enantiomer, the imaginary line joining the two spherical lobes is rotated $-7°$ $(+7°)$ from the long axis of the molecule. Moreover, the S- (or Ƨ-) shaped central lobe features a darker line, which is not aligned with the two spherical lobes. Thus, based on
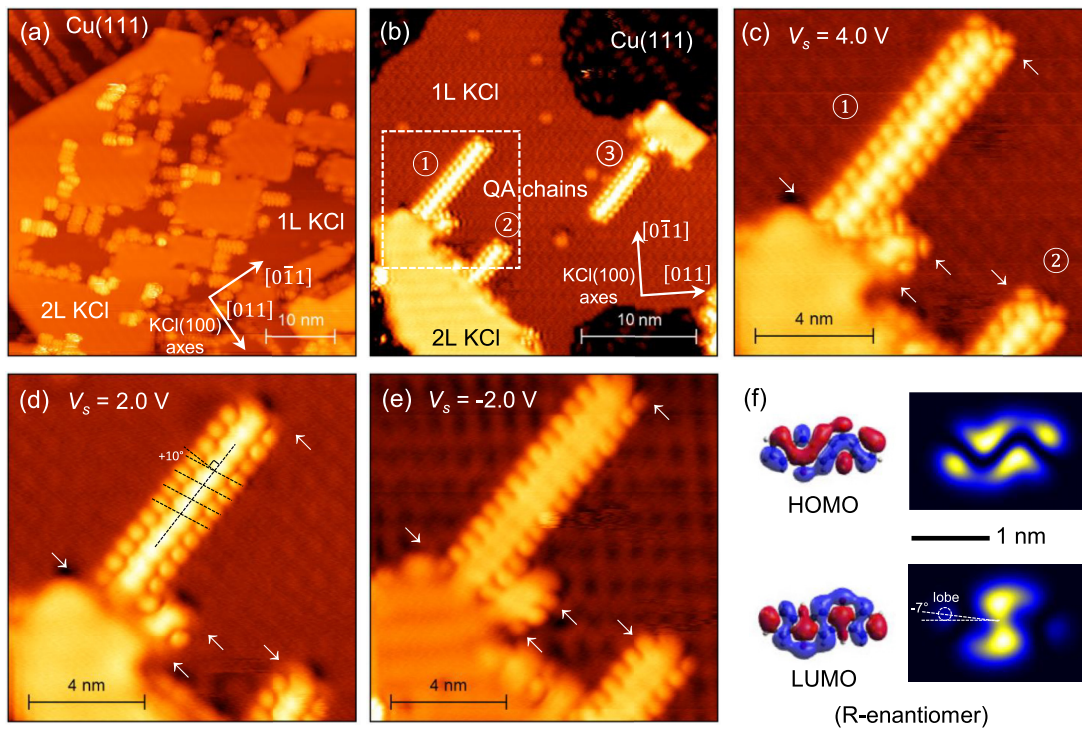
FIG. 3. (a)–(e) STM topography images of QA molecules deposited on an ultrathin KCl film grown on Cu(111), featuring 1L- and 2L-thick KCl areas. STM parameters: (a)–(c) 4.0 V, 4 pA; (d) 2.0 V, 4 pA; (e) −2.0 V, 4 pA. The images shown in (c) to (e) correspond to the same area as framed in dotted line in (b) and show QA chains on 1L-thick KCl. The white arrows in (c) to (e) are guides for the eye to help visualize the position of the molecules. (f) DFT calculations (details available in Ref. [41]) of the frontier orbitals of the neutral molecule and corresponding maps of their partial density of states at constant height. Panel (f) is adapted with permission from Ref. [41].

the relative position of its lobes in the STM image, one can determine the chirality of a given QA molecule and its in-plane orientation. Using this method, we identify the molecules in chains ① and ② in Fig. 3(b) as the L-enantiomer and the molecules in chain ③ as the R-enantiomer. In chain ③, the imaginary line joining the two spherical lobes of each QA molecule is perpendicular to the chain axis, whereas in chains ① and ②, this line is rotated $+(10 \pm 1)°$ from the perpendicular to the chain axis. Knowing the chirality of QA molecules, we deduce that the QA long axis is rotated $+(7 \pm 1)°$ from

the perpendicular to the chain axis in chain ③, and $+(3 \pm 1)°$ in chains ① and ②. Based on these deductions and on the measured intermolecular distances, we make models for the molecular arrangement of the QA chains. The models shown in Figs. 5(a) and 5(b) correspond to chains ① and ② and to chain ③, respectively. For the sake of simplicity, only three QA molecules of each chain are represented. As stated above, chains ①, ②, and ③ have their axis at $+(2.5 \pm 1.0)°$ from the KCl [001] direction. Hence, QA molecules have their long axis oriented at $+(9.5 \pm 2.0)°$ from the KCl [010] direction
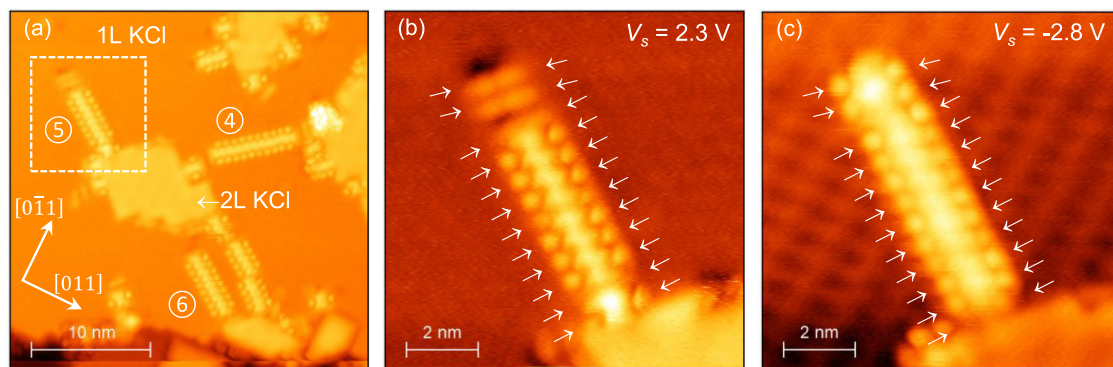

FIG. 4. (a)–(c) STM topography images of QA molecules deposited on an ultrathin KCl film grown on Cu(111), featuring 1L- and 2L-thick KCl areas. STM parameters: (a) 3.0 V, 4 pA; (b) 2.3 V, 4 pA; (c) −2.8 V, 4 pA. The images shown in (b) and (c) correspond to the same area as framed in dotted line in (a) and show a QA chain on 1L-thick KCl. The white arrows in (b) and (c) are guides for the eye to help visualize the position of the molecules.
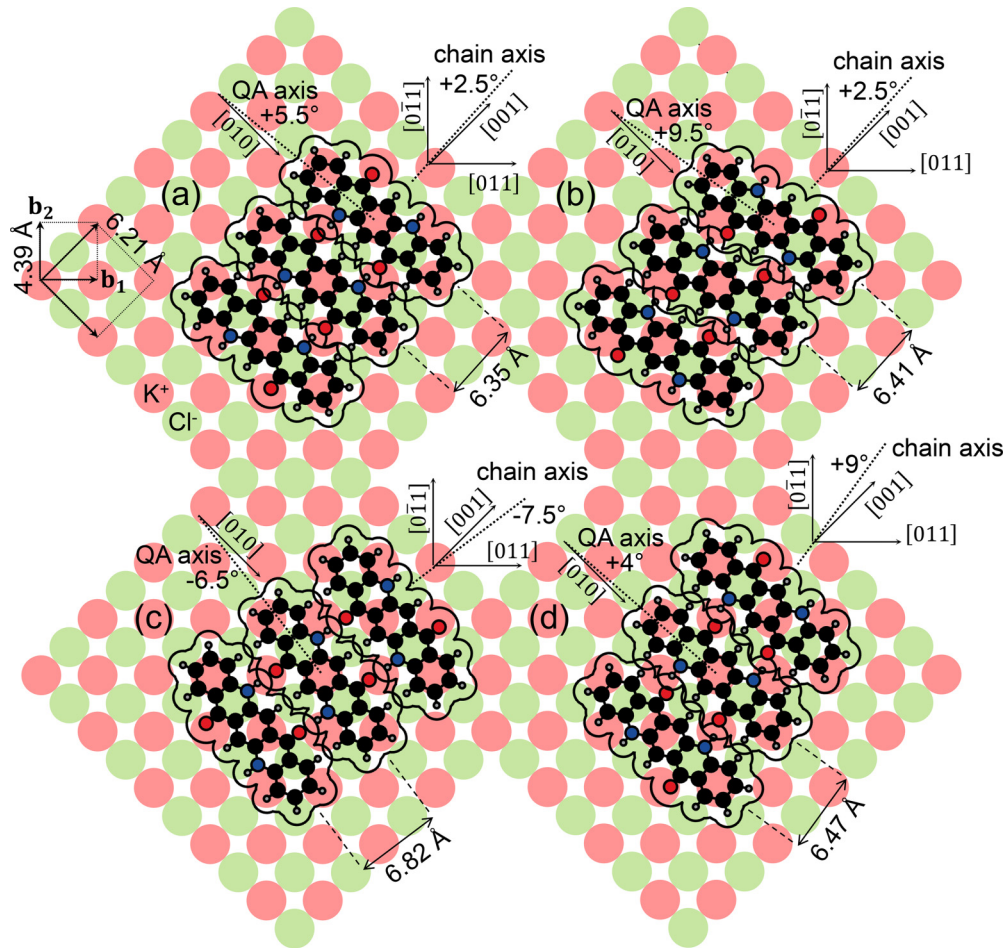
FIG. 5. Models for the molecular arrangement of the QA chains on 1L-thick KCl/Cu(111) shown in Figs. 3 and 4: (a) chains ① and ② in Fig. 3, (b) chain ③ in Fig. 3, (c) chain ④ in Fig. 4, and (d) chains ⑤ and ⑥ in Fig. 4.

in chain ③ [see Fig. 5(b)], and $+(5.5 \pm 2.0)°$ in chains ① and ② [see Fig. 5(a)].

As shown in Fig. 3, QA molecules at nonequivalent positions in the chain may have distinct STM contrasts, from which the chirality of the molecules can also be deduced. In Fig. 3(c), the molecules located at both ends of the three QA chains exhibit a different STM contrast than the other molecules of the chain, which is dependent on the applied sample bias. At $V_s = 4.0$ V, the image of these molecules reproduces the DFT-calculated partial density of states of the highest occupied molecular orbital (HOMO). As shown in Fig. 3(f), the partial density of states of the HOMO of the R-enantiomer features a ∧-shaped central dark line, which (for symmetry reasons) is ∧-shaped for the L-enantiomer. In this way, we confirm that the molecules at both ends of the chains shown in Fig. 3(c) have the same chirality as the other molecules of these chains. This is consistent with the previously reported property that straight QA chains are enantiopure, because the presence of the two enantiomers in the same chain yields lateral shifts of the molecules with respect to the chain axis [33].

At $V_s = 2.0$ V [Fig. 3(d)], the rodlike image of the molecules at the chain ends and their comparatively lower STM height indicate that electrons tunnel from tip to sample through the electronic band gap of the molecules. Based on the comparison of Figs. 3(c) and 3(d), we find that this rod is oriented parallel to the long axis of QA. At $V_s = -2.0$ V [Fig. 3(e)], all the molecules in the chains exhibit the same STM contrast, which makes it possible to determine the number of molecules constituting the chain without ambiguity. (Note that the calculations here are primarily used to help determine the orientation of the QA molecules and that a full interpretation of the appearance of molecules in terms of molecular orbitals is beyond the scope of this work.)

Similar observations can be made for the QA chains on 1L-thick KCl shown in Fig. 4. The three longest chains, labeled from ④ to ⑥ in Fig. 4(a), comprise 12, 12, and 10 QA molecules, respectively. Using the same method as introduced above, we identify the R-enantiomer in chain ④ and the L-enantiomer in chains ⑤ and ⑥, except the two QA molecules at the top end of chain ⑤ in Fig. 4(b), which are of the R-enantiomer. To the precision of the measurements, chains ⑤ and ⑥ have the same in-plane orientation, with the chain axis rotated $+(9 \pm 1)°$ from the KCl [010] direction, and the same intermolecular distance, i.e., 644 ± 11 pm for chain ⑤ and 647 ± 3 pm for chain ⑥. In both chains, the QA long axis is rotated $-(5 \pm 1)°$ from the perpendicular to the chain axis, i.e., $+(4 \pm 2)°$ from the KCl [001] direction. This is in contrast with chain ④, for which we measure the chain axis orientation at $-(7.5 \pm 0.5)°$ from the KCl [001] direction and

a comparatively larger (by about 5%) intermolecular distance of 682 ± 3 pm. [Note that the other shorter QA chains observed in Fig. 4(a) exhibit intermolecular distances ranging from 641 ± 6 pm to 662 ± 8 pm.] In chain ④, the QA long axis is rotated $+(1 \pm 1)°$ from the perpendicular to the chain axis, i.e., $-(6.5 \pm 1.5)°$ from the KCl [010] direction. The models shown in Figs. 5(c) and 5(d) correspond to chain ④ and to chains ⑤ and ⑥, respectively.

In Fig. 4, we observe comparable bias-dependent effects on the STM contrast as in Fig. 3. Several molecules exhibit a rodlike STM contrast at $V_s = 2.3$ V and $V_s = 3.0$ V, which changes into the LUMO-like contrast at $V_s = -2.8$ V. We speculate that different STM contrasts result from the nonequivalent electronic and dielectric environments of the molecules in the chains, as demonstrated for other systems, e.g., PTCDA clusters on bilayer NaCl/Ag(111) [80]. Moreover, the STM images presented in this work reveal the presence of atomic defects in the KCl films [see the dark spots in Figs. 2(d) and 2(e) and the bright spots in Fig. 3(b)]. QA molecules may be adsorbed on such defects or interact with them, which may result in energy shifts of the molecular orbitals or in a different charge state of the molecule [41].

In the models shown in Fig. 5, the adsorption site of the QA chains on KCl is chosen arbitrarily, based on simple considerations about electrostatic interactions between the functional groups of QA and the K^+ and Cl^- ions of the underlying KCl layer. Namely, the chains are laterally positioned to have the oxygen atoms of the carbonyl groups (which carry negative partial charges) on top of potassium cations. Naturally, all the molecules may not have such energy-favorable adsorption sites in chains that are longer than three molecules. Nevertheless, these simple models help understand the experimentally observed dependence of the intermolecular distance on the in-plane orientation of the molecules relative to the chain axis. When the QA long axis is orthogonal to the chain axis, e.g., in Fig. 5(c), the functional groups of the neighboring molecules perfectly face each other. Thus, these groups form hydrogen bonds that are oriented parallel to the chain axis. When the QA long axis is not orthogonal to the chain axis, i.e., in the three other cases shown in Fig. 5, these functional groups are laterally shifted by a few tens of picometers with respect to each other. As a result, the formed hydrogen bonds are tilted with respect to the direction of the chain axis. Assuming that the hydrogen bond length is the same in all models shown in Fig. 5, tilted hydrogen bonds yield shorter intermolecular distances.

2. QA chains on 2L- and 3L-thick KCl

Figure 6 shows STM images of QA molecules deposited on 2L- and 3L-thick KCl areas of KCl islands grown on Cu(111). We find that QA spontaneously arranges in 1D molecular chains on both 2L- and 3L-thick KCl areas. Straight linear chains coexist with "broken" chains, i.e., QA chains that exhibit some degree of disorder. Such disorder may either result from insufficient mobility of the molecules on KCl at the considered substrate temperatures or be due to the presence of both enantiomers of the adsorbed prochiral molecule. Straight linear chains of QA molecules either grow starting
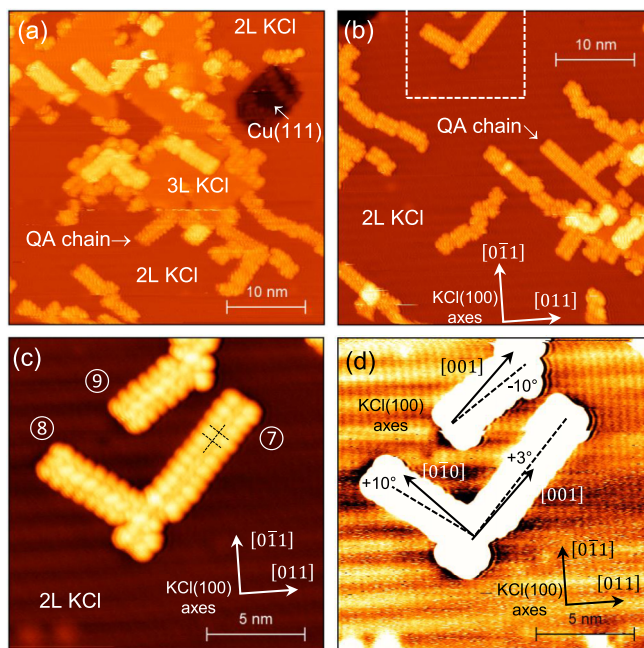

FIG. 6. (a)–(d) STM topography images of QA molecules deposited on an ultrathin KCl film grown on Cu(111), featuring 2L- and 3L-thick KCl areas. STM parameters: (a), (b) sample bias 4.6 V, set-point current 2 pA; (c), (d) 4.0 V, 4 pA. The images shown in (c) and (d) correspond to the same area as framed in dotted line in (b). In the image shown in (d), the vertical scale is intentionally saturated, in order to highlight the moiré pattern and the atomic resolution on KCl.

from 2L/3L KCl step edges or on flat terraces without the assistance of KCl step edges. The QA chain arrowed in Fig. 6(b) comprises 16 QA molecules and is oriented parallel to the [010] axis of the underlying KCl surface.

Some angular dispersion around the KCl ⟨100⟩ directions is observed for the orientation of the other QA chains in Fig. 6(b). For example, the axis of the chains labeled from ⑦ to ⑨ in Fig. 6(c) is rotated $+3°$, $+10°$, and $-10°$ from the closest KCl ⟨100⟩ directions, respectively [see Fig. 6(d)]. For the two QA chains rotated by $\pm 10°$ (chains ⑧ and ⑨), we measure similar intermolecular distances, i.e., 669 ± 15 pm and 661 ± 15 pm, respectively. To the experimental uncertainty, this equals the intermolecular distance measured for QA chains directly grown on Cu(111), i.e., 666 ± 10 pm. The QA chain rotated by $+3°$ (chain ⑦) features a comparatively shorter intermolecular distance of 641 ± 15 pm.

As shown in Fig. 6(c), QA chains with two different contrasts can be found in the STM images. At 4.0 V and 4 pA, the side lobes are apparently higher than the central lobes of chain ⑦, whereas the contrary is observed for chains ⑧ and ⑨. Despite lower spatial resolution (due to the larger scan size), we observe that the QA chains on 2L- and 3L-thick KCl shown in Figs. 6(a) and 6(b) exhibit either one or the other of these two contrasts. In Fig. 6(c), we find a correlation between the observed STM contrast and the intermolecular distance measured along the chain axis. Thus, we infer that distinct STM contrasts result from a different overlapping of
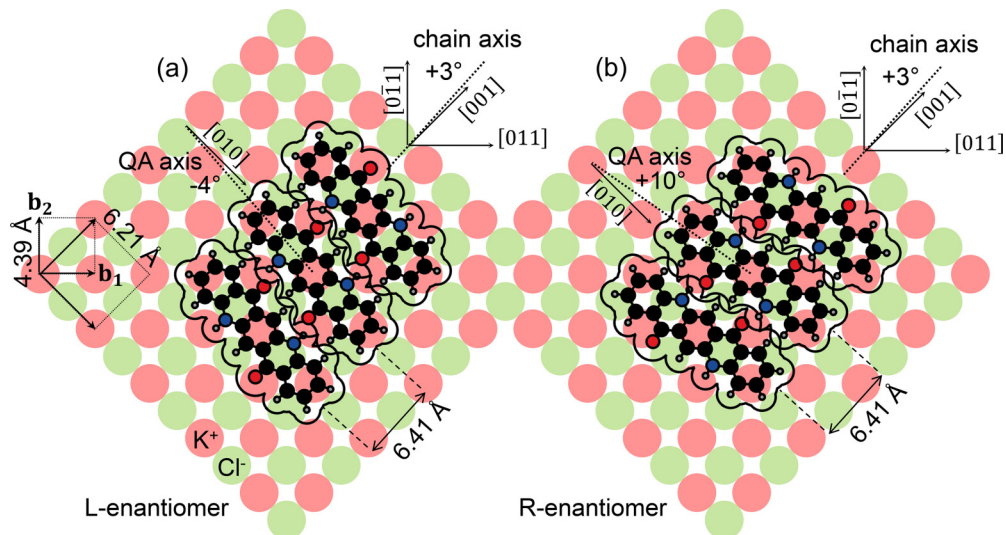
FIG. 7. (a), (b) Models for the molecular arrangement of a QA chain on 2L-thick KCl/Cu(111) shown in Fig. 6 and labeled chain ⑦. QA molecules are assumed to adsorb on KCl as the L-enantiomer in (a) and as the R-enantiomer in (b). For the sake of simplicity, only three QA molecules per chain are represented. The adsorption site of QA on KCl is chosen arbitrarily.

the orbitals of the neighboring molecules, due to different intermolecular distances.

In the STM images, the apparent width of the QA molecules increases with the thickness of the underlying KCl film. This is due to the convolution with the shape of the STM tip apex. For the STM parameters used here, the STM height of QA molecules increases with the number of KCl atomic layers. As a result, these convolution effects are the strongest for QA on 3L-thick KCl and the weakest for QA on 1L-thick KCl. This makes it more difficult to distinguish the different lobes of each molecule in a QA chain on 2L- and 3L-thick KCl, as compared to 1L-thick KCl. In particular, the chirality of the adsorbed molecules and their in-plane orientation cannot be deduced without ambiguity for QA chains ⑧ and ⑨ in Fig. 6. However, we clearly see in Fig. 6(c) that the imaginary line joining the spherical lobes of the QA molecules in chain ⑦ is orthogonal to the chain axis. Thus, we infer the two possible models shown in Fig. 7, each of which corresponding to one of the two enantiomers. In both models, the neighboring QA molecules are laterally shifted by the same distance (but in opposite directions), which results in the same angular tilt (in absolute value) of the hydrogen bonds with respect to the direction of the chain axis. In agreement with our observations for QA chains on 1L-thick KCl, we find that intermolecular distances of about 6.4 Å are measured when the hydrogen bonds are not oriented parallel to the chain axis.

3. Discussion on the absence of commensurate structures

As shown in Fig. 8, the growth of homochiral QA chains along the KCl ⟨100⟩ directions could be commensurate (i.e., with all QA molecules at equivalent adsorption sites) if the intermolecular distance along the QA chain axis equaled the KCl lattice parameter, which we measure to be 6.21 Å at 78 K. However, such a short intermolecular distance is not experimentally observed. This confirms that QA chain growth on

KCl/Cu(111) is incommensurate, within the range of investigated growth parameters and KCl film thicknesses. Figure 8 shows two different molecular arrangements having the same intermolecular distance of 6.21 Å, but differing in the in-plane orientation of the molecules. In Fig. 8(a), we consider the case where the QA long axis is orthogonal to the chain axis, which is the case where the hydrogen bonds would be the shortest. This arrangement is not experimentally observed, presumably because the hydrogen bond length would be too short to be stable. In Fig. 8(b), the in-plane orientation of the QA molecules is such that the oxygen atom of the carbonyl groups is equidistant from the closest hydrogen atoms of the neighboring molecule, which is the case where the hydrogen bonds would be the longest. This arrangement implies a comparatively shorter distance between the long axes (and thus a stronger spatial overlapping) of the neighboring molecules, which possibly explains why it is not experimentally observed either. To sum up, we infer from the models shown in Fig. 8 that the commensurate growth of QA chains along the KCl ⟨100⟩ directions is hindered by QA-QA intermolecular interactions, either due to the (too short) length of the hydrogen bonds or the (too short) distance between the long axes of neighboring molecules.

The growth of homochiral QA chains along the KCl ⟨110⟩ directions is not experimentally observed either. As shown in Fig. 9, QA chains oriented parallel to the KCl ⟨110⟩ directions would present a higher-order commensurability with the KCl lattice for an intermolecular distance of $\frac{3}{2\sqrt{2}}$ times the KCl lattice parameter (6.21 Å at 78 K), i.e., 6.59 Å. This value is within the range of experimentally measured intermolecular distances (6.4–6.8 Å). Therefore, we infer that the growth of QA chains oriented along the KCl ⟨110⟩ directions is not hindered by QA-QA intermolecular interactions, but by QA-KCl electrostatic interactions. This may be due to the fact that, in this molecular arrangement of the QA chains, only the second-next-neighbor molecules have equivalent adsorption sites.
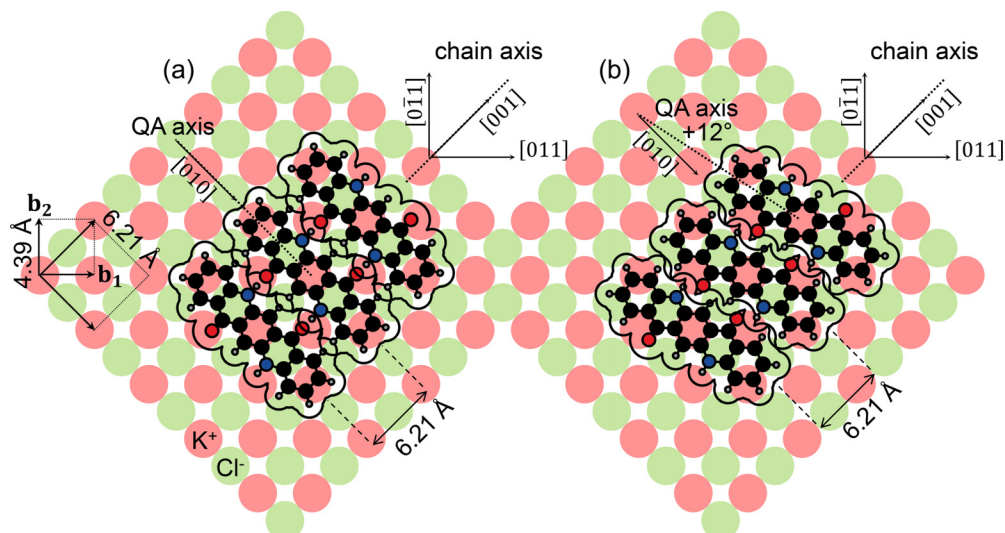
FIG. 8. (a), (b) Hypothetical adsorption models for QA molecules arranged in a 1D chain on the KCl(100) surface, where the chain axis is oriented parallel to a KCl ⟨100⟩ direction and the intermolecular distance is commensurate with KCl lattice parameter (i.e., all QA molecules have identical adsorption sites). The adsorption site of QA on KCl is chosen arbitrarily. The molecular arrangement shown in these models is not experimentally observed.

Overall, our results indicate that the in-plane orientation of the chain axis relative to KCl directions and of the QA long axis with respect to the chain axis is mainly governed by molecule-substrate QA-KCl interactions. These QA-KCl interactions are most likely dominated by the electrostatic interactions between the functional groups of the molecules and the K^+ and Cl^- ions of the underlying KCl layer. The in-plane orientation of QA long axis with respect to the chain axis dictates the orientation of the hydrogen bonds between

neighboring molecules, which determines the intermolecular distance. Finally, we conclude that the experimental difficulties to obtain comparatively long (i.e., several tens of molecules) and straight QA chains on KCl thin films may be mostly due to the kinetics of QA diffusion on KCl and the difficulty to grow such thin films with high surface coverage and low defect (step, hole, and kink) density.

IV. CONCLUSIONS

We have investigated the growth of 1D molecular chains of quinacridone (QA) on ultrathin KCl films on Cu(111) using low-temperature STM in UHV at 78 K. After deposition on Cu(111) partially covered with KCl islands, QA molecules spontaneously arrange into straight homochiral 1D chains both on the bare Cu(111) areas and on 1L-, 2L-, and 3L-thick KCl areas. On KCl, QA chains either nucleate at defects or step edges or grow on terraces without assistance of defects. Irrespective of the in-plane orientation of KCl islands relative to Cu(111), the longest straight QA chains observed in this work are oriented with the chain axis parallel to or rotated less than 10° from the closest KCl ⟨100⟩ direction. The growth of QA chains oriented along the KCl ⟨110⟩ directions is hindered by QA-KCl electrostatic interactions. The measured intermolecular distances for QA chains on KCl/Cu(111) range from 6.4 to 6.8 Å, which is compatible with hydrogen bonds between neighboring flat-lying QA molecules. QA-KCl interactions likely govern the in-plane orientation of the chain axis relative to KCl directions and the in-plane orientation of the QA long axis with respect to the chain axis, whereas QA-QA interactions determine the intermolecular distance. Within the investigated range of growth parameters and KCl film thicknesses, QA chain growth on KCl/Cu(111) is found to be incommensurate.

Our results may help answer the increasing demand for self-assembled nanoscale systems of π-conjugated molecules on thin insulating layers, for the study of emergent physics
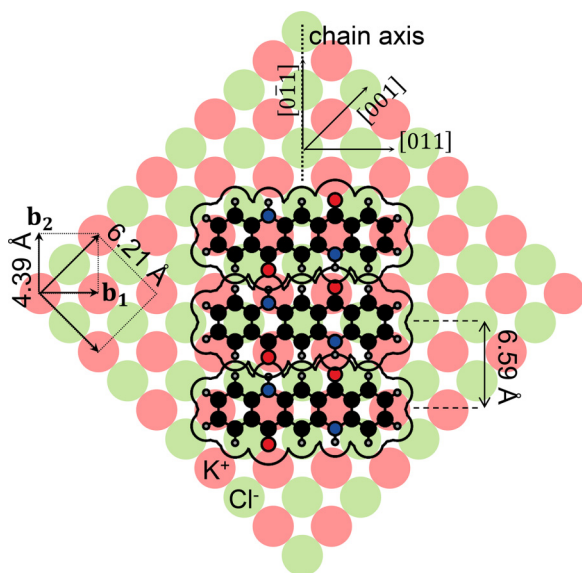

FIG. 9. Hypothetical adsorption model for QA molecules arranged in a 1D chain on the KCl(100) surface, where the chain axis is oriented parallel to a KCl ⟨110⟩ direction. The intermolecular distance is chosen such that all second-nearest-neighbor molecules have identical adsorption sites (i.e., higher-order commensurability). The molecular arrangement shown in this model is not experimentally observed.

in nanophotonics, nanoelectronics, and excitonics. Moreover, the variations in intermolecular distance and relative orientation of the molecules observed from one chain to another offer unique possibilities to study the effect of these geometric parameters on the optical, electronic, vibrational, and excitonic properties of such molecular chains. Furthermore, QA chain growth on KCl/Cu(111) being incommensurate, this system makes it possible to study how an inhomogeneous dielectric and electronic environment alters the coherent coupling of the molecules in a chain (i.e., exciton delocalization) and possibly leads to exciton localization effects. We envisage that such investigations can be carried out on the nanometer scale using tip-enhanced Raman scattering (TERS) and photoluminescence (TEPL) and STM-induced luminescence (STML) spectroscopy and microscopy. Finally, we believe that the fine variations in the molecular arrangement of QA chains reported in this article are of technological relevance for the performance of future QA-based (and possibly QA/alkali halide based) devices.

[1] J. V. Barth, G. Constantini, and K. Kern, Nature (London) **437**, 671 (2005).

[2] D. P. Goronzy, M. Ebrahimi, F. Rosei, Arramel, Y. Fang, S. De Feyter, S. L. Tait, C. Wang, P. H. Beton, A. T. S. Wee, P. S. Weiss, and D. F. Perepichka, ACS Nano **12**, 7445 (2018).

[3] L. Xing, Z. Peng, W. Li, and K. Wu, Acc. Chem. Res. **52**, 1048 (2019).

[4] S. Clair and D. G. de Oteyza, Chem. Rev. **119**, 4717 (2019).

[5] E. Geagea, F. Palmino, and F. Cherioux, Chemistry **4**, 796 (2022).

[6] S.-Q. Zhang, L.-X. Cheng, Z.-L. Gong, W.-B. Duan, B. Tu, Y.-W. Zhong, and Q.-D. Zeng, Langmuir **35**, 6571 (2019).

[7] A. Jeindl, J. Domke, L. Hörmann, F. Sojka, R. Forker, T. Fritz, and O. T. Hofmann, ACS Nano **15**, 6723 (2021).

[8] S. Aeschlimann, S. V. Bauer, M. Vogtland, B. Stadtmüller, M. Aeschlimann, A. Floris, R. Bechstein, and A. Kühnle, Nat. Commun. **11**, 6424 (2020).

[9] T. R. Rusch, M. Hammerich, R. Herges, and O. M. Magnussen, Chem. Commun. **55**, 9511 (2019).

[10] S. A. Svatek, J. Kerfoot, A. Summerfield, A. S. Nizovtsev, V. V. Korolkov, T. Taniguchi, K. Watanabe, E. Antolín, E. Besley, and P. H. Beton, Nano Lett. **20**, 278 (2020).

[11] E. Mohammadifar, V. Ahmadi, M. F. Gholami, A. Oehrl, O. Kolyvushko, C. Nie, I. S. Donskyi, S. Herziger, J. Radnik, K. Ludwig, C. Böttcher, J. P. Rabe, K. Osterrieder, W. Azab, R. Haag, and M. Adeli, Adv. Funct. Mater. **31**, 2009003 (2021).

[12] Y. Zhao, M. Gobbi, L. E. Hueso, and P. Samorí, Chem. Rev. **122**, 50 (2022).

[13] E. D. Głowacki, L. Leonat, M. Irimia-Vladu, R. Schwödiauer, M. Ullah, H. Sitter, S. Bauer, and N. S. Sariciftci, Appl. Phys. Lett. **101**, 023305 (2012).

[14] E. D. Głowacki, M. Irimia-Vladu, M. Kaltenbrunner, J. Gsiorowski, M. S. White, U. Monkowius, G. Romanazzi, G. P. Suranna, P. Mastrorilli, T. Sekitani, S. Bauer, T. Someya, L. Torsi, and N. S. Sariciftci, Adv. Mater. **25**, 1563 (2013).

[15] A. Cahlík, J. Hellerstedt, J. I. Mendieta-Moreno, M. Švec, V. M. Santhini, S. Pascal, D. Soler-Polo, S. I. Erlingsson, K. Výborný, P. Mutombo, O. Marsalek, O. Siri, and P. Jelínek, ACS Nano **15**, 10357 (2021).

[16] A. S. Davydov and N. I. Kislukha, Phys. Status Solidi B **59**, 465 (1973).

[17] M.-a. Morikawa, M. Yoshihara, T. Endo, and N. Kimizuka, J. Am. Chem. Soc. **127**, 1358 (2005).

[18] S. K. Saikin, A. Eisfeld, S. Valleau, and A. Aspuru-Guzik, Nanophotonics **2**, 21 (2013).

[19] T. Brixner, R. Hildner, J. Köhler, C. Lambert, and F. Würthner, Adv. Energy Mater. **7**, 1700236 (2017).

[20] R. Pant and S. Wüster, Phys. Chem. Chem. Phys. **22**, 21169 (2020).

[21] S. B. Anantharaman, K. Jo, and D. Jariwala, ACS Nano **15**, 12628 (2021).

[22] K. Kreger, H.-W. Schmidt, and R. Hildner, Electron. Struct. **3**, 023001 (2021).

[23] L. Varvelo, J. K. Lynd, and D. I. G. Bennett, Chem. Sci. **12**, 9704 (2021).

[24] M. Böhringer, K. Morgenstern, W.-D. Schneider, R. Berndt, F. Mauri, A. De Vita, and R. Car, Phys. Rev. Lett. **83**, 324 (1999).

[25] J. Weckesser, A. De Vita, J. V. Barth, C. Cai, and K. Kern, Phys. Rev. Lett. **87**, 096101 (2001).

[26] J. V. Barth, J. Weckesser, G. Trimarchi, M. Vladimirova, A. De Vita, C. Cai, H. Brune, P. Günter, and K. Kern, J. Am. Chem. Soc. **124**, 7991 (2002).

[27] Q. Chen and N. V. Richardson, Nat. Mater. **2**, 324 (2003).

[28] J. Schnadt, E. Rauls, W. Xu, R. T. Vang, J. Knudsen, E. Lægsgaard, Z. Li, B. Hammer, and F. Besenbacher, Phys. Rev. Lett. **100**, 046103 (2008).

[29] M. Yu, N. Kalashnyk, R. Barattin, Y. Benjalal, M. Hliwa, X. Bouju, A. Gourdon, C. Joachim, E. Lægsgaard, F. Besenbacher, and T. R. Linderoth, Chem. Commun. **46**, 5545 (2010).

[30] J. Lipton-Duffin, J. Miwa, S. G. Urquhart, G. Contini, A. Cossaro, L. Casalis, J. V. Barth, L. Floreano, A. Morgante, and F. Rosei, Langmuir **28**, 14291 (2012).

[31] M. Koepf, F. Chérioux, J. A. Wytko, and J. Weiss, Coord. Chem. Rev. **256**, 2872 (2012).

[32] T. Wagner, M. Györök, D. Huber, P. Zeppenfeld, and E. D. Głowacki, J. Phys. Chem. C **118**, 10911 (2014).

[33] N. Humberg, R. Bretel, A. Eslam, E. Le Moal, and M. Sokolowski, J. Phys. Chem. C **124**, 24861 (2020).

[34] F. Trixler, T. Markert, M. Lackinger, F. Jamitzky, and W. M. Heckl, Chem. Eur. J. **13**, 7785 (2007).

[35] K. Stallberg, A. Namgalies, S. Chatterjee, and U. Höfer, J. Phys. Chem. C **126**, 12728 (2022).

[36] J. Repp, G. Meyer, S. M. Stojković, A. Gourdon, and C. Joachim, Phys. Rev. Lett. **94**, 026803 (2005).

[37] F. Aguilar-Galindo, M. Zapata-Herrera, S. Díaz-Tendero, J. Aizpurua, and A. G. Borisov, ACS Photonics **8**, 3495 (2021).

[38] H. Imada, K. Miwa, M. Imai-Imada, S. Kawahara, K. Kimura, and Y. Kim, Nature (London) **538**, 364 (2016).

[39] Y. Zhang, Y. Luo, Y. Zhang, Y.-J. Yu, Y.-M. Kuang, L. Zhang, Q.-S. Meng, Y. Luo, J.-L. Yang, Z.-C. Dong, and J. G. Hou, Nature (London) **531**, 623 (2016).

[40] B. Doppagne, M. C. Chong, E. Lorchat, S. Berciaud, M. Romeo, H. Bulou, A. Boeglin, F. Scheurer, and G. Schull, Phys. Rev. Lett. **118**, 127401 (2017).

[41] S. Jiang, T. Neuman, R. Bretel, A. Boeglin, F. Scheurer, E. Le Moal, and G. Schull, Phys. Rev. Lett. **130**, 126202 (2023).

[42] B. Yang, G. Chen, A. Ghafoor, Y. Zhang, Y. Zhang, Y. Zhang, Y. Luo, J. Yang, V. Sandoghdar, J. Aizpurua, Z. Dong, and J. G. Hou, Nat. Photon. **14**, 693 (2020).

[43] H. Imada, M. Imai-Imada, K. Miwa, H. Yamane, T. Iwasa, Y. Tanaka, N. Toriumi, K. Kimura, N. Yokoshi, A. Muranaka, M. Uchiyama, T. Taketsugu, Y. K. Kato, H. Ishihara, and Y. Kim, Science **373**, 95 (2021).

[44] A. Rosławska, K. Kaiser, M. Romeo, E. Devaux, F. Scheurer, S. Berciaud, T. Neuman, and G. Schull, arXiv:2305.13157.

[45] A. Kabakchiev, K. Kuhnke, T. Lutz, and K. Kern, ChemPhysChem **11**, 3412 (2010).

[46] K. Kuhnke, V. Turkowski, A. Kabakchiev, T. Lutz, T. S. Rahman, and K. Kern, ChemPhysChem **19**, 277 (2018).

[47] T. Leoni, L. Nony, E. Zaborova, S. Clair, F. Fagès, F. Para, A. Ranguis, C. Becker, and C. Loppacher, Phys. Rev. B **104**, 205415 (2021).

[48] M. Pivetta, F. Patthey, M. Stengel, A. Baldereschi, and W.-D. Schneider, Phys. Rev. B **72**, 115404 (2005).

[49] H.-C. Ploigt, C. Brun, M. Pivetta, F. Patthey, and W.-D. Schneider, Phys. Rev. B **76**, 195404 (2007).

[50] G. Cabailh, C. R. Henry, and C. Barth, New J. Phys. **14**, 103037 (2012).

[51] A. Husseen, S. Le Moal, H. Oughaddou, G. Dujardin, A. Mayne, and E. Le Moal, Phys. Rev. B **96**, 235418 (2017).

[52] Y. Luo, G. Chen, Y. Zhang, L. Zhang, Y. Yu, F. Kong, X. Tian, Y. Zhang, C. Shan, Y. Luo, J. Yang, V. Sandoghdar, Z. Dong, and J. G. Hou, Phys. Rev. Lett. **122**, 233901 (2019).

[53] E. F. Paulus, F. J. J. Leusen, and M. U. Schmidt, CrystEngComm **9**, 131 (2007).

[54] C. Wang, Z. Zhang, and Y. Wang, J. Mater. Chem. C **4**, 9918 (2016).

[55] S. E. Shaheen, B. Kippelen, N. Peyghambarian, J.-F. Wang, J. D. Anderson, E. A. Mash, P. A. Lee, N. R. Armstrong, and Y. Kawabe, J. Appl. Phys. **85**, 7939 (1999).

[56] H. Yanagisawa, J. Mizuguchi, S. Aramaki, and Y. Sakai, Jpn. J. Appl. Phys. **47**, 4728 (2008).

[57] T. V. Pho, P. Zalar, A. Garcia, T.-Q. Nguyen, and F. Wudl, Chem. Commun. **46**, 8210 (2009).

[58] T. Yang, Y. Liu, J. Qiu, H. Zhang, F. Li, and Y. Wang, Chem. Eng. J. **432**, 134405 (2022).

[59] M. Shen, X. Zhao, L. Han, N. Jin, S. Liu, T. Jia, Z. Chen, and X. Zhao, Chem. A: European J. **28**, e202104137 (2022).

[60] L. S. Hung, C. W. Tang, and M. G. Mason, Appl. Phys. Lett. **70**, 152 (1997).

[61] L. S. Hung, R. Q. Zhang, P. He, and G. Mason, J. Phys. D: Appl. Phys. **35**, 103 (2002).

[62] C. J. Brabec, S. E. Shaheen, C. Winder, N. S. Sariciftci, and P. Denk, Appl. Phys. Lett. **80**, 1288 (2002).

[63] T. M. Brown, R. H. Friend, I. S. Millard, D. J. Lacey, T. Butler, J. H. Burroughes, and F. Cacialli, J. Appl. Phys. **93**, 6159 (2003).

[64] L. Ma and Y. Yang, Appl. Phys. Lett. **85**, 5084 (2004).

[65] S. Wang, P. K. L. Chan, C. Wah Leung, and X. Zhao, RSC Adv. **2**, 9100 (2012).

[66] H. Wang, P. Amsalem, G. Heimel, I. Salzmann, N. Koch, and M. Oehzelt, Adv. Mater. **26**, 925 (2014).

[67] S. Wan, G. Zhang, J. Niederhausen, D. Wu, Q. Wang, B. Sun, T. Song, and S. Duhm, Appl. Phys. Lett. **118**, 241601 (2021).

[68] M. Vogelgesang, Ultrathin KCl films on Cu(110) and Cu(111) studied by low-temperature scanning tunneling microscopy, Ph.D. thesis, EPFL, Lausanne, 2005, doi:10.5075/epfl-thesis-3352.

[69] C. Loppacher, U. Zerweck, and L. M. Eng, Nanotechnology **15**, S9 (2004).

[70] M. Müller, J. Ikonomov, and M. Sokolowski, Surf. Sci. **605**, 1090 (2011).

[71] S. Fölsch, A. Helms, and K. H. Rieder, Appl. Surf. Sci. **162-163**, 270 (2000).

[72] A. Riemann, S. Fölsch, and K. H. Rieder, Phys. Rev. B **72**, 125423 (2005).

[73] I. Beinik, C. Barth, M. Hanbücken, and L. Masson, Sci. Rep. **5**, 8223 (2015).

[74] S. A. Burke, J. M. Topple, and P. Grütter, J. Phys.: Condens. Matter **21**, 423101 (2009).

[75] H. Karacuban, S. Koch, M. Fendrich, T. Wagner, and R. Möller, Nanotechnology **22**, 295305 (2011).

[76] D. Nečas and P. Klapetek, Open Phys. **10**, 181 (2012).

[77] C. A. Schneider, W. S. Rasband, and K. W. Eliceiri, Nat. Methods **9**, 671 (2012).

[78] See Supplemental Material at https://link.aps.org/supplemental/10.1103/PhysRevB.108.125423 for the STM images of NaCl islands on Cu(111) and the QA chains on 2L-thick KCl islands oriented with the KCl ⟨110⟩ directions at 15° from the Cu ⟨110⟩ directions.

[79] D. B. Sirdeshmukh, L. Sirdeshmukh, and K. G. Subhadra, *Alkali Halides: A Handbook of Physical Properties*, Springer Series in Materials Science (Springer, Berlin, 2001).

[80] K. A. Cochrane, A. Schiffrin, T. S. Roussy, M. Capsoni, and S. A. Burke, Nat. Commun. **6**, 8312 (2015).